RESEARCH ARTICLE

**ADVANCED
ELECTRONIC
MATERIALS**

Open Access

Check for updates

www.advelectronicmat.de

Tailoring Magnetic Anisotropy in Ultrathin Cobalt by Surface Carbon Chemistry

Carlo Alberto Brondin,* Sukanya Ghosh, Saikat Debnath, Francesca Genuzio, Pietro Genoni, Matteo Jugovac, Stefano Bonetti, Nadia Binggeli, Nataša Stojić, Andrea Locatelli, and Tevfik Onur Menteş*

The ability to manipulate magnetic anisotropy is essential for magnetic sensing and storage tools. Surface carbon species offer cost-effective alternatives to metal-oxide and noble metal capping layers, inducing perpendicular magnetic anisotropy in ultrathin ferromagnetic films. Here, the different mechanisms by which the magnetism in a few-layer-thick Co thin film is modified upon adsorption of carbon monoxide (CO), dispersed carbon, and graphene are elucidated. Using X-ray microscopy with chemical and magnetic sensitivity, the in-plane to out-of-plane spin reorientation transition in cobalt is monitored during the accumulation of surface carbon up to the formation of graphene. Complementary magneto-optical measurements show weak perpendicular magnetic anisotropy (PMA) at room temperature for dispersed carbon on Co, while graphene-covered cobalt exhibits a significant out-of-plane coercive field. Density-functional theory (DFT) calculations show that going from CO/Co to C/Co and to graphene/Co, the magnetocrystalline and magnetostatic anisotropies combined promote out-of-plane magnetization. Anisotropy energies weakly depend on carbidic species coverage. Instead, the evolution of the carbon chemical state from carbidic to graphitic is accompanied by an exponential increase in the characteristic domain size, controlled by the magnetic anisotropy energy. Beyond providing a basic understanding of the carbon-ferromagnet interfaces, this study presents a sustainable approach to tailor magnetic anisotropy in ultrathin ferromagnetic films.

1. Introduction

Magnetic anisotropy in ultrathin ferromagnetic films reflects the broken symmetries at the film surface and interface. In many cases, the competition between bulk and surface contributions to the anisotropy energy results in spin-reorientation transitions (SRT) as a function of film thickness.[1,2] In general, such transitions depend on surface structure and chemistry. Therefore, surface adsorbates provide a sensitive means to tune the film's magnetic properties.

Among the plethora of different adsorbate/ferromagnetic material combinations, polymorphs of carbon on cobalt films are of particular interest. In fact, almost all relevant studies point to an enhancement of Co PMA in the presence of carbon and to the existence of exotic magnetic domain structures in ultrathin Co films with PMA.[3,4] Notable examples of PMA enhancement were obtained by covering the Co surface with graphene,[5,6] C_{60},[7] and CO.[8] The adsorption site of CO was reported to have an important

C. A. Brondin, S. Bonetti
Dipartimento di Scienze Molecolari e Nanosistemi
Università Ca' Foscari di Venezia
Via Torino 155, Venezia, Venezia Mestre 30172, Italia
E-mail: carloalberto.brondin@elettra.eu

C. A. Brondin, F. Genuzio[+], M. Jugovac, A. Locatelli, T. O. Menteş
Elettra Sincrotrone Trieste SCpA
Strada Statale 14 - km 163,5 in Area Science Park, Trieste, Basovizza 34149, Italia
E-mail: tevfik.mentes@elettra.eu

S. Ghosh
Department of Physics and Astronomy
Uppsala University
Ångströmlaboratoriet, Lägerhyddsvägen
1 Box 516, Uppsala 75120, Sweden

S. Debnath
Department of Physics
M. V. College
HXC8+588, Charitra Van, Buxar, Bihar 802101, India

P. Genoni[++]
Dipartimento di Fisica e Astronomia
CIMaINa, Università degli Studi di Milano
Via Celoria 16, Milano 20133, Italia

2300579 (1 of 8)

**ADVANCED
SCIENCE NEWS**

www.advancedsciencenews.com

**ADVANCED
ELECTRONIC
MATERIALS**

www.advelectronicmat.de

role in PMA.[9] Moreover, the dissociation of CO and the subsequent accumulation of carbidic and graphitic carbon on Co were shown to result in the strengthening of PMA.[10–12]

On the other hand, graphene (gr) on ultrathin Co films obtained by CO dissociation enhances the SRT thickness up to only ≈6 monolayers (ML),[12] in variation from the initial reports of Co intercalated between gr/Ir(111) resulting in an SRT thickness between 12 and 15 ML.[5,6] Indeed, the surface configuration is not the only determining factor. The substrate interface[13] and stacking within the Co film[14] are proven to be equally important to magnetic anisotropy as the particular surface adlayer. The interface between Co and the heavy metal substrate is particularly important in light of the tendency towards alloying between 3d metal overlayers and 5d substrates (with a decreasing tendency from Pt and Ir toward Re and W[15]). Such alloying may have an impact on the film magnetization, as it was demonstrated in the case of Co/Ir(111).[16] Therefore, a reliable comparison of different C adspecies necessarily needs to be sought after using identical Co film configurations.

In this work, we carry out a comparative study of the effect of CO, C, and gr on ultrathin Co films on Re(0001). In particular, we experimentally and theoretically address the magnitude of PMA differences between molecular CO, carbidic C, and graphene adsorbed on Co films close to the SRT thickness. Magnetic domains visualized by laterally-resolved X-ray magnetic circular dichroism (XMCD) are used to monitor qualitative changes in PMA, whereas magneto-optical Kerr effect (MOKE) measurements provide a more quantitative and less-invasive means to evaluate magnetic properties. DFT calculations are used to model the experimentally observed structures and indicate the contributions to the Co magnetic anisotropy energy for the different surface adlayers considered. Importantly, the calculated anisotropy energies give insight into the role of different contributions to magnetic anisotropy in determining the morphology of magnetic domains.

2. Results

The evolution of magnetic domains in an ultrathin Co film grown on Re(0001) under CO dose and X-ray exposure is seen in the X-ray magnetic circular dichroism photoemission electron microscopy (XMCD-PEEM) images in **Figure 1**. The relatively-high Co deposition temperature (520 K) leads to a quasi layer-by-layer growth with micron-sized regions of well-defined thicknesses and with predominantly hcp stacking.[17] For the sample displayed in Figure 1, the thickness varies between 2 and 5 ML as determined by the quantum oscillations in the low-energy electron microscopy (LEEM) reflectivity curves[18,19] and indicated on the LEEM image in Figure 1a. Figure 1b shows the magnetic domains in Co upon adsorption of two Langmuirs of CO. The irregular in-plane magnetic domains of the pristine film evolve into

regular stripe patterns for four layer and five layer regions after dosing several Langmuirs of CO as seen in Figure 1c.

Stripe domains are known to arise in films with out-of-plane magnetization due to the competition between the short-range domain wall energy and the long-range dipolar interaction.[20] Thus, the appearance of magnetic stripes in Figure 1 is associated with the reorientation of magnetization along the surface normal. Additional CO exposure leads to an increase in the period of the magnetic stripe domains as seen in Figure 1d, which suggests a strengthening of the PMA.[21] On the other hand, CO adsorption at room temperature on similar Co films is reported not to enhance the PMA based on the particular adsorption site of the CO molecule.[22,23]

Notably, there is no conflict between these reports and the data displayed in Figure 1, as the X-ray irradiation applied in our XMCD measurements is known to promote the dissociation of CO molecules, leading to carbon accumulation on the surface.[10,11] Thus, the exposure to X-rays during the XMCD measurements in Figure 1 and the subsequent dissociation of CO is crucial in inducing the PMA in Co. Indeed, in our previous studies we showed that electron and X-ray-induced CO dissociation can be used to pattern the magnetic anisotropy.[10]

In order to evaluate the dependence of PMA on the quantity and the chemical state of carbon, we employ MOKE. This technique allows studying surface magnetization through the polarization analysis of visible light in reflection geometry.[24–26] The utilization of visible light prevents any changes to the chemical state in particular of the CO molecule, making a comparative measurement of different chemical adspecies possible. The out-of-plane hysteresis loops measured in polar geometry are presented in **Figure 2**. Data are acquired from three different C-based adspecies on a four-layer thick cobalt film grown on Re(0001). Hard-axis response of 4 ML pristine Co is shown in Figure 2a, with the inclined baseline dominated by the paramagnetic response from the optical system. An identical curve is found for $\sqrt{3} \times \sqrt{3}$ R30° CO/Co as can be seen in Figure 2b. This indicates that magnetization still lies in-plane. Cracking the CO by electron beam leaves carbidic C on the surface. We ensured by C 1s XPS that the amount of C was equal to the CO-covered surface, that is, 1/3 ML. For this carbidic surface, Figure 2c shows the beginning of an out-of-plane hysteresis loop with a coercivity around 5 ± 2 mT. Further loading with carbon by subsequent cracking of CO leads to a complete graphene layer upon annealing at 680 K. The loop acquired (Figure 2d) clearly indicates out-of-plane magnetization consistent with the literature.[5]

Experimental data displayed in Figures 1 and 2 qualitatively point out the magnetization variations induced by different carbon adspecies. In order to evaluate the strength of PMA changes for the surfaces considered in Figure 2, we carried out DFT calculations using slabs shown in **Figure 3**a–e that model the samples measured in Figure 2 (except the 2/3 ML carbon covered surface).

The calculated magnetocrystalline contribution (MCA) to the magnetic anisotropy energy (MAE) is shown in **Figure 4**a. Note that, as the slab model does not include the Re substrate, only the changes in MCA values between different adsorbate or surface configurations are meaningful and therefore we report the MCA values relative to the pristine cobalt surface. The calculated total values of MCA for the different slabs are presented in Supporting

S. Bonetti
Department of Physics
Stockholm University
Roslagstullsbacken 21, Stockholm 114 21, Sweden

N. Binggeli, N. Stojić
The Abdus Salam International Centre for Theoretical Physics
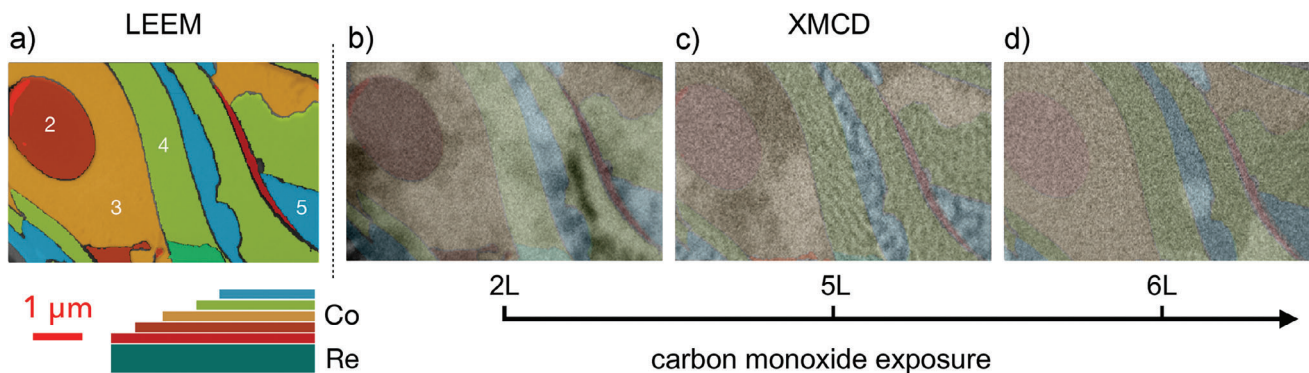ICTP - Strada Costiera 11, Trieste 34151, Italia

ADVANCED
SCIENCE NEWS

www.advancedsciencenews.com

ADVANCED
ELECTRONIC
MATERIALS

www.advelectronicmat.de

Figure 1. a) Color-coded LEEM image of a multi-thickness cobalt film grown on Re(0001). Numeric labels mark the number of Co ML in that specific region. b–d) XMCD-PEEM images acquired at the Co L$_3$ edge as a function of CO dose indicated in Langmuirs below each image. The dichroic images correspond to the difference between two opposite X-ray circular polarization states.

Information Figure S2a, Supporting Information. Regarding the relative MCA contribution, molecular CO adsorption slightly enhances the in-plane anisotropy. On the other hand, the carbidic carbon resulting from the dissociation of CO strengthens the tendency towards out-of-plane magnetization. This trend is even more pronounced for graphene on Co.

Even though carbon–cobalt interaction is weaker for gr/Co compared to the carbidic surface, there is a strong orbital hybridization between C and Co also in the case of graphene, which is reflected in mixed C-Co states near the Fermi level with single spin polarization.[27] The enhancement of MCA in the case of graphene on Co also derives from the hybridization between Co d and carbon p orbitals. In particular, we find that the trends in the MCA are mainly controlled by the changes in the Co d$_{z^2}$ projected density of states (PDOS) and the d$_{z^2}$ - d$_{yz}$ orbital coupling. For graphene on Co, the Co minority-spin d$_{z^2}$ PDOS is drastically reduced close to the Fermi energy due to the hybridization with the C π (p$_z$) orbital, and results in a large increase in the MCA. In addition, the hybridization increases the Co d$_{z^2}$ majority PDOS at energies somewhat below the Fermi energy, which also increases the MCA. This is consistent with the analysis given in ref. [6] of

the MCA changes produced by graphene in gr/Co heterostructures. Instead, in the case of carbidic C, all three p orbitals are occupied at E_F and C atoms are found in different adsorption sites with respect to Co atoms. Thus, Co d$_{z^2}$ orbitals are not strongly involved anymore in the hybridization at around E_F, and there is no reduction of d$_{z^2}$ PDOS in the minority spin channel, which leaves the MCA virtually unchanged. More detailed information on the relation between MCA and orbital hybridization can be found in Section S3, Supporting Information.

In thin films, shape anisotropy energy (SAE), that is, the dipolar contribution to the MAE, should also be taken into account. SAE always favors in-plane magnetization to reduce magnetic stray fields. The calculated values of SAE for C/Co configurations are given in Figure 4b. We keep the same reference as for the MCA values, presenting the SAE values relative to the pristine Co surface. This results in positive variations of SAE with respect to the Co slab, while the total values of the calculated slab SAE, shown in Figure S2b, Supporting Information, are always negative. In our calculations, the total value of the SAE for the pristine six-layer Co film amounts to −89 µeV per Co atom and constitutes the lowest value of SAE among all the configurations
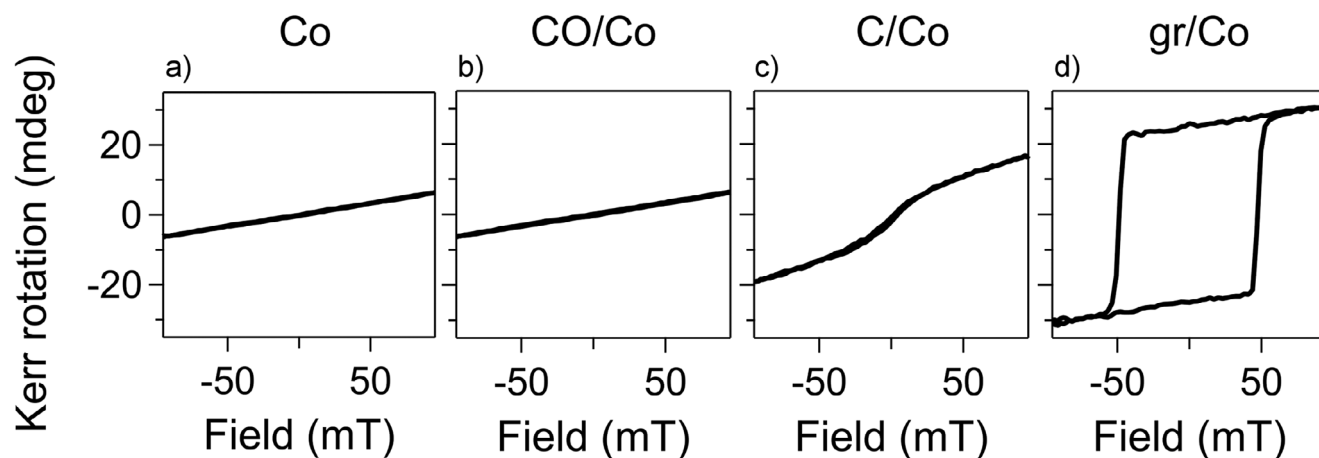

Figure 2. Polar MOKE hysteresis loops of 4 ML thick Co on Re(0001) measured for different surface configurations: a) clean surface, b) $\sqrt{3} \times \sqrt{3}$ R30° CO/Co, c) e-beam dissociated CO on Co, d) gr/Co. The corresponding LEED patterns are shown in the Supporting Information (Figure S1, Supporting Information).
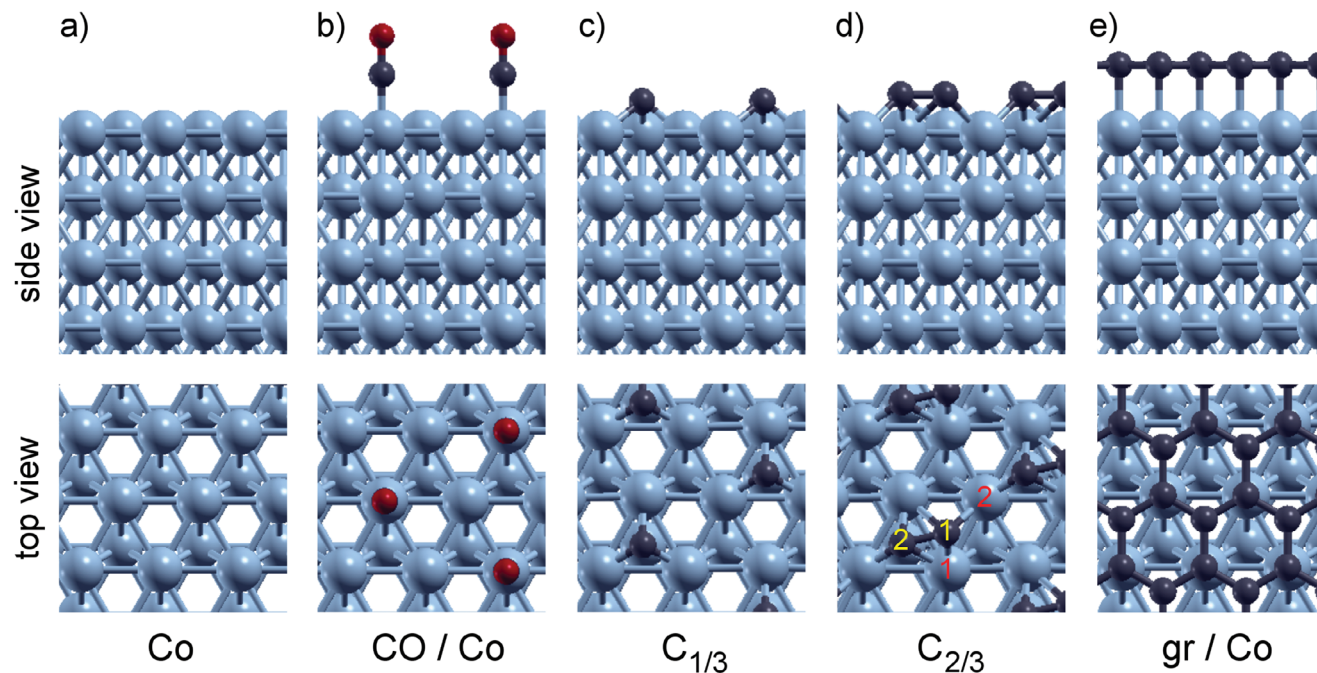
**ADVANCED
SCIENCE NEWS**

www.advancedsciencenews.com

**ADVANCED
ELECTRONIC
MATERIALS**

www.advelectronicmat.de

Figure 3. Top and side views of the DFT calculated structures based on a six-layer symmetric Co slab: a) clean surface; b) $\sqrt{3} \times \sqrt{3}$ R30° CO/Co; c) C (1/3 ML)/Co; d) C (2/3 ML)/Co; e) gr/Co. Light blue balls stand for Co atoms, black for C, and red for O atoms. The numeric labels of atom in (d) are used in the text and in Table 1.

considered. We note that our calculated SAE values are in good agreement with the values obtained from the well-known expression for SAE from the continuum theory, $-1/2\mu_0\langle M_s\rangle^2$, where $\langle M_s\rangle$ stands for the average spin moment per unit volume and μ_0 is the permeability of free space. In fact, for the pristine Co SAE, this yields about -90 μeV per Co atom.

As can be seen in Figure 4b, the SAE values for different Co surface configurations do not follow the same trend as the MCA. In particular, molecular CO and carbidic C induce a weaker in-plane anisotropy in terms of SAE, contrary to the graphene layer, which leaves the dipolar energy of the pristine cobalt film nearly unchanged. Variation of SAE is related to the change in the magnetic moment of the Co surface atoms, induced by the interaction between Co and carbon adspecies. The magnetic moments of the Co atoms of the outermost Co layer, as well as those of the adsorbed species and the corresponding adsorption energy and C–Co distances, are presented in **Table 1**.

Strong reduction of the magnetic moment in Co from the value of 1.67 μ_B is related to a strong interaction between carbon and cobalt resulting in a closer atomic distance and larger adsorption energy, as can be seen in Table 1. Reduction of the magnetic moment is observed to be dependent on the C–Co bonding, where the Co atoms directly bonded to C exhibit a lower magnetic moment compared to those without any coordination with carbon. In the case of $\sqrt{3} \times \sqrt{3}$ R30° CO structure in Figure 3b, Co atoms directly below the CO molecule present a much smaller magnetic moment (0.76 μ_B) than those further away (1.67 μ_B). Carbidic C coordinates with all the surface Co in the same manner. Thus, magnetic moments are uniformly reduced (0.94 μ_B). In contrast, an uneven reduction in magnetic mo-

ments is observed in the surface covered by 2/3 ML of carbides shown in Figure 3d, as Co atoms that are bonded to adjacent dimers display a smaller suppression (0.82 μ_B) of the magnetic moment compared to those placed between two dimers (0.35 μ_B)

Table 1. DFT calculated magnetic moments (m) of the outermost Co atoms and of the adsorbate atoms; average C–Co distance (d_{C-Co}) and adsorption energies (E_{ads}) for the four structures shown in Figure 3. In the case of CO/Co, Co(1) refers to atoms that are directly below the CO molecule and Co(2) to the rest of the outermost Co atoms. In the case of C(2/3 ML)/Co surface carbon and cobalt atoms are not equivalent, and the numeric labels in Figure 3d establish the connection between the atoms and the corresponding values in the table.

		m (μ_B)	d_{C-Co} (Å)	E_{ads} (eV per C atom)
Co		1.67	–	–
CO/Co	C :	−0.05		
	O :	−0.03	1.70	−2.47
	Co(1) :	0.76		
	Co(2) :	1.69		
C$_{(1/3)}$/Co	C :	−0.15	1.74	−8.32
	Co :	0.94		
C$_{(2/3)}$/Co	C(1) :	−0.05		
	C(2) :	−0.03	1.87	−8.35
	Co(1) :	0.82		
	Co(2) :	0.35		
gr/Co	C$_{top}$:	0.05		
	C$_{hollow}$:	−0.05	2.06	−0.95
	Co :	1.47		

ADVANCED
SCIENCE NEWS

www.advancedsciencenews.com

ADVANCED
ELECTRONIC
MATERIALS
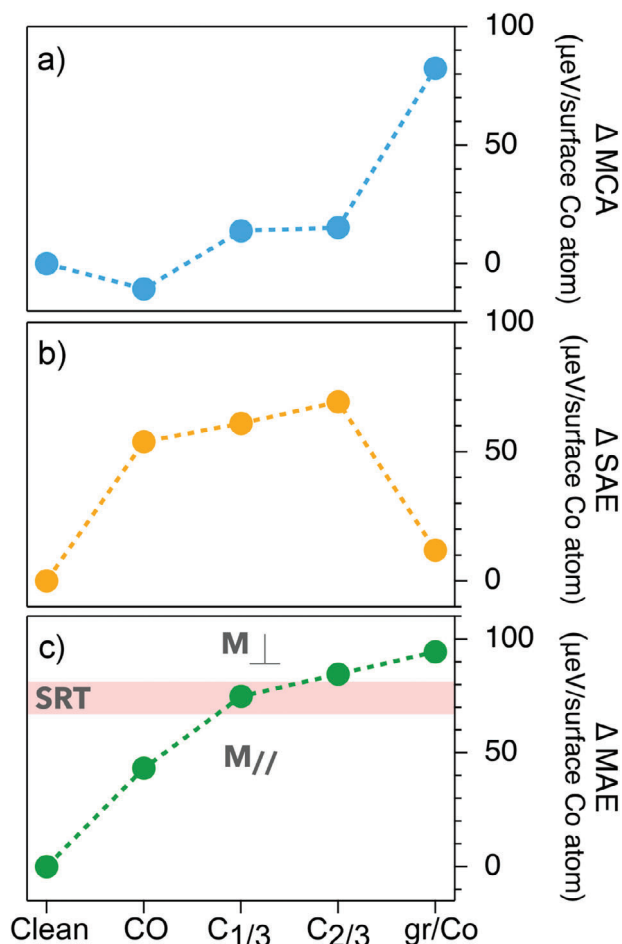Open Access

www.advelectronicmat.de

Figure 4. Variations in a) magnetocrystalline and b) dipolar contributions to the calculated magnetic anisotropy energy are shown with respect to pristine Co. c) Change in total MAE (MCA+SAE) for the configurations sketched in Figure 3. Note that an increase in the values of MAE indicates a heightened tendency toward PMA. Pink band in (c) indicates the position of the experimental SRT based on Figure 2.

The extra carbon atom causes a further reduction in the average magnetic moment of surface Co atoms and subsequently weakens the dipolar anisotropy by ≈4%. On the other hand, the MCA value calculated for 2/3 ML C/Co is within 0.45 µeV of the value for 1/3 ML C/Co. Therefore, we can conclude that beyond a certain C coverage, accumulating further carbidic carbon nearly leaves unchanged the MCA, whereas it slightly increases the tendency for out-of-plane magnetization due to a small reduction in the SAE.

The onset and the evolution of the magnetic stripes with increasing carbon coverage are shown in **Figure 5**. The magnetic domains were assessed by XMCD-PEEM and the amount and chemical state of the carbon by core-level XPS. The XMCD image series shown in Figure 5a displays the Co magnetic domain distribution for increasing carbon coverage upon CO dose and subsequent dissociation through e-beam. Figure 5 a1 displays typical in-plane magnetic domains for the clean surface, consistent with the MOKE hysteresis loop presented in Figure 2a. At 0.34 ML carbon, magnetic stripes can be discerned (Figure 5 a2), indicating that the Co magnetization reorients from in-plane to out-of-plane. Increasing the carbon coverage leads to an increment in the stripe period, keeping the labyrinth configuration. As the period increases, the regular stripe morphology is lost, as seen in the last two images (4 and 5) presented in Figure 5a. Nevertheless, the magnetization preserves its out-of-plane orientation, as confirmed by the presence of only two contrast levels in the XMCD images, and the average domain size can still be measured.

The amount and chemical state of carbon on the surface were evaluated using C 1s XPS core-level peak fitting with two main components at around 285.0 eV and at 283.5 eV corresponding to graphitic and carbidic C, respectively.[28] The change in the relative magnitude of the two components can be seen in Figure 5b as a function of the total carbon coverage, which we evaluate by quantitatively comparing the XPS C $1s$ spectrum with that of a full graphene layer taken as a reference. It is important to notice that carbidic and graphitic carbon accumulates on the surface with increasing carbon coverage due to progressive CO dissociation under e-beam. This enrichment of graphitic carbon accelerates at around 1 ML and levels off as the graphene layer is almost complete, obtained by the subsequent thermal transformation of carbides into graphene (corresponding to about 2 ML in units of Co atomic density).

Chemical changes in the carbon overlayer are reflected in the evolution of the out-of-plane stripe period plotted on a logarithmic scale in Figure 5c. Domain size remains relatively unchanged for the first three data points, for which the carbon is predominantly carbidic. Upon the beginning of graphitization, the stripe period quickly rises and slows down as the graphene layer is completed, closely following the graphitic carbon in the XPS data displayed in Figure 5b.

As mentioned previously, the formation of stripes is a result of the competition between the energy associated with domain walls and the dipolar interaction. This gives rise to an equilibrium stripe period that depends exponentially on the MAE, the exchange energy, J, and the long-range contribution to the dipolar energy, Ω.[21,29,30] Importantly, in the vicinity of the spin reorientation transition, at which the MAE vanishes, the relative change in MAE dominates over those in J and Ω. This causes the MAE to be the controlling parameter for the domain size in the vicinity

(corresponding to the atoms 1 and 2 denoted in Figure 3d). On the other hand, upon graphitization C–Co bond weakens, and the Co magnetic moment (1.47 μ_B) nearly recovers its pristine value.

Changes in total MAE, found from the sum of Δ(MCA) and Δ(SAE), are shown in Figure 4c. The horizontal pink bar in the plot indicates the threshold for the experimentally-observed SRT, obtained from Figure 2. Data in Figure 4c show the progressive trend to out-of-plane magnetization going from pristine Co, CO/Co, C/Co, to graphene on Co. Regarding MCA, gr/Co is considerably stronger than the other surfaces in terms of promoting out-of-plane magnetization. The same is found in the total MAE, although the difference between graphene and the other carbon species is substantially reduced due to the dipolar energy, which is suppressed due to the quenched surface Co magnetic moments in CO/Co and C/Co. Considering two carbidic configurations allows us to compare the effect of carbidic coverage on the magnetic anisotropy. The two carbon atoms placed in the same $\sqrt{3} \times \sqrt{3}$ R30° unit cell bind together strongly to form a dimer, whose atomic configuration can be seen in Figure 3d.
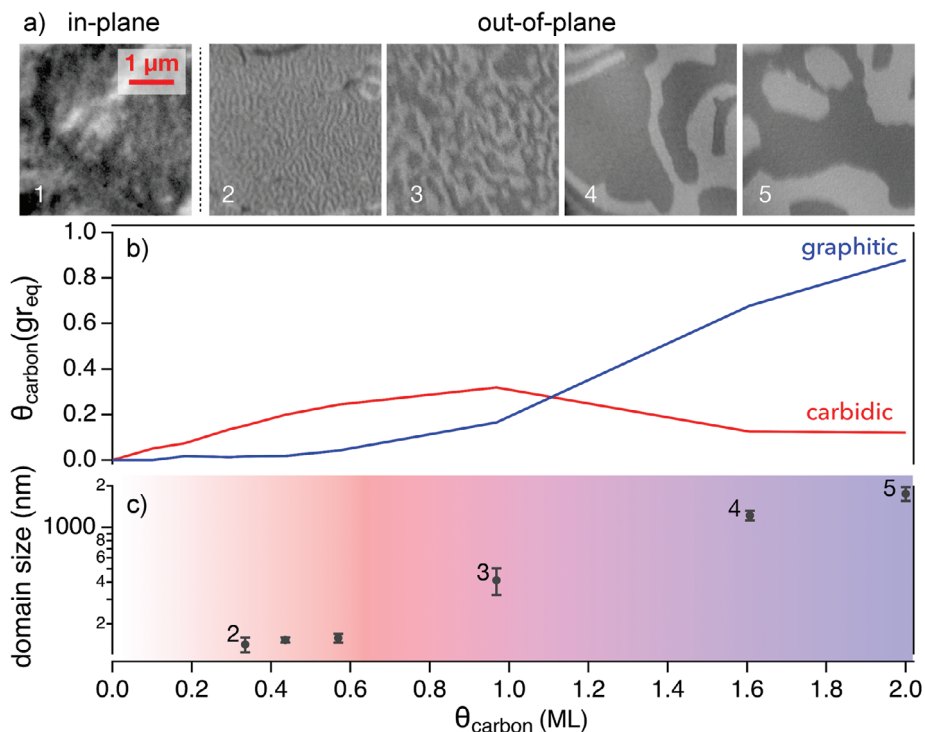
Figure 5. a) XMCD-PEEM images of a 4 ML Co film acquired at the Co L_3 edge for increasing CO dose. b) Evolution of carbon species extracted from the C 1s core-level XPS peak fitting is shown as a function of the total carbon coverage. The horizontal axis is in monolayer units of Co surface atomic density, whereas the vertical axis is normalized to the signal from a complete single graphene layer. The XPS fits are shown in Figure S4, Supporting Information. c) Period of magnetic stripe domains as a function of total carbon coverage. The methodology used to estimate the domain period in XMCD-PEEM images is explained in Section S5, Supporting Information. The numeric labels near the data points indicate the corresponding XMCD images in panel (a), and the background color coding reflects the chemical state of carbon based on the plot in panel (b).

of the spin reorientation transition (configurations 3, 4, and 5 in Figure 5c).

The relatively constant domain size for the carbidic adsorbates can be understood to be a consequence of thermal fluctuations and temperature-dependent universal scaling laws, as the pattern period was shown to approach a constant value in the critical regime of the phase transition.[31,32] Therefore, we conclude that the points in Figure 5c for 4 ML Co and for carbide coverage varying from ≈0.3 ML to about ≈0.6 ML all lie within the critical regime of the spin reorientation transition, thus resulting in the nearly constant stripe period.

3. Conclusion

We experimentally and theoretically studied the spin reorientation in ultrathin Co films induced by adsorbed carbon species. DFT calculations, modeling the selected interfaces, reflect the changes to the magnetocrystalline and magnetostatic dipolar contributions to the magnetic anisotropy energy. In particular, the magnetocrystalline term progressively enhances out-of-plane magnetization, going from molecular CO to surface carbide to graphene on cobalt. However, this tendency is somewhat lessened due to the dipolar anisotropy, which is relatively weaker for the carbide and molecular CO_covered Co surfaces due to a reduction in the surface Co magnetic moment. Experimental results indicate a spin reorientation transition at about 4 ML thickness for the carbide-covered Co film. Remarkably, the ob-

served microscopic domain morphology remains nearly invariant upon increasing carbidic carbon coverage, which is attributed to the stripe period approaching a constant value within the critical regime near the spin reorientation transition. From the carbidic to the graphene-covered-Co regime, instead, the domain size exhibits an exponential behavior controlled by the magnetic anisotropy energy. Our results reveal how the perpendicular magnetic anisotropy and domain morphology develop upon carbon accumulation and subsequent graphitization on the Co ultrathin film surface.

4. Experimental Section

Cathode Lens Microscopy: The experiments were carried out at the Nanospectroscopy beamline (Elettra synchrotron, Trieste), where a Spectroscopic Photoemission and Low Energy Electron Microscope (SPELEEM III, Elmitec GmbH)[33] is installed. SPELEEM provides information on the morphology and structure by elastically backscattered electrons (LEEM), and on the chemical, electronic, and magnetic properties by photoemitted electrons (XPEEM).[34] The kinetic energy of the emitted electrons is selected by tuning a voltage bias applied to the sample typically called as *start voltage*. The lateral resolution of the SPELEEM is 10 nm in LEEM mode and 25 nm in PEEM mode, and the energy resolution is 100 meV.[34]

Magneto-Optical Kerr Effect: MOKE characterization was carried out in an ancillary UHV experimental chamber,[35] providing the possibility to exchange samples with the SPELEEM setup without breaking the vacuum. The electromagnet available in the MOKE chamber is capable of generating magnetic fields up to 140 mT.

**ADVANCED
SCIENCE NEWS**

www.advancedsciencenews.com

**ADVANCED
ELECTRONIC
MATERIALS**

www.advelectronicmat.de

The sample could be positioned to measure either a longitudinal or polar magnetic response. A CW He–Ne laser at 633 nm was used as the light source. Changes in polarization were determined by means of a polarization modulation technique involving a photoelastic modulator PEM.[36]

Theoretical Methods: In order to perform structural optimizations of the adsorbate systems, compare their energy stability, magnetic properties, and evaluate MCA energies, spin-polarized fully relativistic density functional theory (DFT) calculations were performed. Plane-wave basis sets were employed as implemented in the ab initio simulation package Quantum ESPRESSO.[37] The exchange and correlation between electrons were treated using the local density approximation (LDA) with the Perdew–Zunger (PZ) functional.[38] The ion-electron interactions were described by the projector-augmented plane-wave potentials.[39] The cutoffs for kinetic energy and charge density for the basis sets were 55 and 550 Ry, respectively. The Brillouin zone was sampled using the Γ-centered Monkhorst–Pack k-point grid of $48 \times 48 \times 1$. The adsorbate systems on Co were described by supercells consisting of six layers of Co(0001), an adsorbate layer (C, Co, and graphene) at each side of the slab and a vacuum layer of 18–20 Å. All the adsorbates were described by a $\sqrt{3} \times \sqrt{3}R30°$ lateral cell. Optimized lattice parameter of Co of 2.42 Å, which is 3% smaller than the experimental value was used. To describe graphene on Co(0001), C atoms were placed in the lowest-energy adsorption sites; on-top and fcc sites. The adsorption sites of CO and C on Co were also optimized in the calculations.

The magnetocrystalline anisotropy energy was obtained by computing the difference in total energies between the parallel and perpendicular orientations of the spin axis:

$$\text{MCA} = E_{\parallel} - E_{\perp} \tag{1}$$

The magnetic dipolar energy, E_{dip}, is evaluated as a sum of magnetic dipolar interaction energies over all pairs of atoms i and j separated by a distance $\mathbf{r}_{ij}$:

$$E_{\text{dip}} = \frac{\mu_0}{8\pi} \sum_{j \neq i} \left[\frac{m_i m_j}{r_{ij}^3} - \frac{3(m_i r_{ij})(m_j r_{ij})}{r_{ij}^5} \right] \tag{2}$$

where μ_0 denotes permeability of free space and $\mathbf{m}_i$ calculated atomic magnetic moment of the atom i. E_{dip} was calculated by fixing the axis of magnetization along the in-plane and out-of-plane spin orientations. Then, the shape anisotropy energy was evaluated by taking the difference between those two orientations:

$$\text{SAE} = E_{\text{dip}\parallel} - E_{\text{dip}\perp} \tag{3}$$

More than 200 lateral cells had been considered, and checked that SAE was converged. The authors employed their own code to perform the summation in Equation (2), using the magnetic moments and distances obtained from the DFT calculations.

Sample Preparation: All the samples presented in this work were prepared in the SPELEEM chamber. The base pressure during all the preparation stages was below 2×10^{-10} mbar, which was sufficient to maintain a clean Co surface in the experimental time frame, making unwanted C contamination negligible compared to the carbon coverages considered in the relevant C-covered surfaces. The cleaning procedure of the Re(0001) single crystal consisted in Ar$^+$ sputtering at 2 kV, $P_{\text{Ar}} = 2 \times 10^{-5}$ mbar, followed by multiple cycles of annealing between 750–1250 K in 1×10^{-6} mbar of molecular oxygen. In order to desorb oxygen the sample was flash annealed at above 2300 K. The surface cleanliness was confirmed by the sharp (1×1) LEED pattern. Cobalt was deposited by an e-beam evaporator from a 99.995% Co rod at a rate of ≈ 0.2 ML min^{-1}. The sample in Figure 1 was obtained by depositing Co while keeping the sample temperature at 520 K. For all the other preparations, the first Co layer was deposited at 620 K and the remaining ones at room temperature. The crystalline order of the Co film was improved by post-annealing at 530 K. Note that the high growth temperature of the first Co layer also ensured that there

were no further changes at the Co–Re interface during the graphitization step carried out at similar temperatures. CO adsorption on Co film was performed by dosing CO at room temperature and $P_{\text{CO}} = 1 \times 10^{-6}$ mbar. Beam-induced CO dissociation was accomplished by using a homemade flood gun operating at low energy around 100 V. Following dissociation, the residual CO was desorbed by annealing at about 470 K. Conversion of residual carbides onto graphene was obtained by annealing the near fully carbon covered surface to 680 K.[10]

Supporting Information

Supporting Information is available from the Wiley Online Library or from the author.

Conflict of Interest

The authors declare no conflict of interest.

Data Availability Statement

The data that support the findings of this study are available from the corresponding author upon reasonable request.

[1] D. Sander, *J. Phys.: Condens. Matter* **2004**, *16*, R603.

[2] C. A. F. Vaz, J. A. C. Bland, G. Lauhoff, *Rep. Prog. Phys.* **2008**, *71*, 056501.

[3] O. Boulle, J. Vogel, H. Yang, S. Pizzini, D. de Souza Chaves, A. Locatelli, T. O. Menteş, A. Sala, L. D. Buda-Prejbeanu, O. Klein, M. Belmeguenai, Y. Roussigné, A. Stashkevich, S. Mourad Chérif, L. Aballe, M. Foerster, M. Chshiev, S. Auffret, I. Mihai Miron, G. Gaudin, *Nat. Nanotechnol.* **2016**, *11*, 449.

[4] L. Camosi, J. Peña Garcia, O. Fruchart, S. Pizzini, A. Locatelli, T. O. Menteş, F. Genuzio, J. M. Shaw, H. T. Nembach, J. Vogel, *New J. Phys.* **2021**, *23*, 013020.

[5] N. Rougemaille, A. T. N'Diaye, J. Coraux, C. Vo-Van, O. Fruchart, A. K. Schmid, *Appl. Phys. Lett.* **2012**, *101*, 142403.

[6] H. Yang, A. D. Vu, A. Hallal, N. Rougemaille, J. Coraux, G. Chen, A. K. Schmid, M. Chshiev, *Nano Lett.* **2016**, *16*, 145.

[7] K. Bairagi, A. Bellec, V. Repain, C. Chacon, Y. Girard, Y. Garreau, J. Lagoute, S. Rousset, R. Breitwieser, Y.-C. Hu, Y. C. Chao, W. W. Pai, D. Li, A. Smogunov, C. Barreteau, *Phys. Rev. Lett.* **2015**, *114*, 247203.

**ADVANCED
SCIENCE NEWS**

www.advancedsciencenews.com

**ADVANCED
ELECTRONIC
MATERIALS**
Open Access

www.advelectronicmat.de

[8] T. Yokoyama, D. Matsumura, K. Amemiya, S. Kitagawa, N. Suzuki, T. Ohta, *J. Phys.: Condens. Matter* **2003**, *15*, S537.

[9] D. Matsumura, K. Amemiya, S. Kitagawa, T. Shimada, H. Abe, T. Ohta, H. Watanabe, T. Yokoyama, *Phys. Rev. B* **2006**, *73*, 174423.

[10] P. Genoni, F. Genuzio, T. O. Menteş, B. Santos, A. Sala, C. Lenardi, A. Locatelli, *ACS Appl. Mater. Interfaces* **2018**, *10*, 27178.

[11] F. Genuzio, P. Genoni, T. O. Menteş, B. Santos, A. Sala, C. Lenardi, A. Locatellim, *J. Phys. Chem. C* **2019**, *123*, 8360.

[12] F. Genuzio, T. O. Menteş, A. Locatelli, *IEEE Trans. Magn.* **2019**, *55*, 2300504.

[13] S. M. Valvidares, J. Dorantes-Dávila, H. Isern, S. Ferrer, G. M. Pastor, *Phys. Rev. B* **2010**, *81*, 024415.

[14] M. Blanco-Rey, P. Perna, A. Gudin, J. M. Diez, A. Anadón, P. Olleros-Rodríguez, L. de Melo Costa, M. Valvidares, P. Gargiani, A. Guedeja-Marron, M. Cabero, M. Varela, C. García-Fernández, M. M. Otrokov, J. Camarero, R. Miranda, A. Arnau, J. I. Cerdá, *ACS Appl. Nano Mater.* **2021**, *4*, 4398.

[15] A. Christensen, A. V. Ruban, P. Stoltze, K. W. Jacobsen, H. L. Skriver, J. K. Nørskov, F. Besenbacher, *Phys. Rev. B* **1997**, *56*, 5822.

[16] J. Drnec, S. Vlaic, I. Carlomagno, C. J. Gonzalez, H. Isern, F. Carlà, R. Fiala, N. Rougemaille, J. Coraux, R. Felici, *Carbon* **2015**, *94*, 554.

[17] M. Parschau, K. Christmann, *Surf. Sci.* **1999**, *423*, 303.

[18] M. S. Altman, W. F. Chung, C. H. Liu, *Surf. Rev. Lett.* **1998**, *05*, 1129.

[19] E. Bauer, *Surface Microscopy with Low Energy Electrons*, Springer, New York, NY **2014**.

[20] J. Stöhr, H. C. Siegmann, *Magnetism*, Springer, Berlin, Heidelberg **2006**.

[21] A. B. Kashuba, V. L. Pokrovsky, *Phys. Rev. B* **1993**, *48*, 10335.

[22] D. Matsumura, T. Yokoyama, K. Amemiya, S. Kitagawa, T. Ohta, *Phys. Scr.* **2005**, *2005*, 583.

[23] D. Matsumura, K. Amemiya, S. Kitagawa, T. Shimada, H. Abe, T. Ohta, H. Watanabe, T. Yokoyama, *Phys. Rev. B* **2006**, *73*, 174423.

[24] J. Kerr, *London Edinburgh Philos. Mag. J. Sci.* **1877**, *3*, 321.

[25] J. Zak, E. R. Moog, C. Liu, S. D. Bader, *J. Magn. Magn. Mater.* **1990**, *89*, 107.

[26] Z. Q. Qiu, S. D. Bader, *Rev. Sci. Instrum.* **2000**, *71*, 1243.

[27] M. Jugovac, I. Cojocariu, F. Genuzio, C. Bigi, D. Mondal, I. Vobornik, J. Fujii, P. Moras, V. Feyer, A. Locatelli, T. O. Menteş, *Adv. Electron. Mater.* **2023**, *9*, 2300031.

[28] M. Jugovac, F. Genuzio, E. Gonzalez Lazo, N. Stojić, G. Zamborlini, V. Feyer, T. O. Menteş, A. Locatelli, C. M. Schneider, *Carbon* **2019**, *152*, 489.

[29] Y. Z. Wu, C. Won, A. Scholl, A. Doran, H. W. Zhao, X. F. Jin, Z. Q. Qiu, *Phys. Rev. Lett.* **2004**, *93*, 117205.

[30] C. Won, Y. Z. Wu, J. Choi, W. Kim, A. Scholl, A. Doran, T. Owens, J. Wu, X. F. Jin, H. W. Zhao, Z. Q. Qiu, *Phys. Rev. B* **2005**, *71*, 224429.

[31] A. D. Stoycheva, S. J. Singer, *Phys. Rev. E* **2001**, *64*, 016118.

[32] T. O. Menteş, A. Locatelli, L. Aballe, E. Bauer, *Phys. Rev. Lett.* **2008**, *101*, 085701.

[33] A. Locatelli, L. Aballe, T. O. Mentes, M. Kiskinova, E. Bauer, *Surf. Interface Anal.* **2006**, *38*, 1554.

[34] T. O. Menteş, G. Zamborlini, A. Sala, A. Locatelli, *Beilstein J. Nanotechnol.* **2014**, *5*, 1873.

[35] F. Genuzio, T. Giela, M. Lucian, T. O. Menteş, C. A. Brondin, G. Cautero, P. Mazalski, S. Bonetti, J. Korecki, A. Locatelli, *J. Synchrotron Radiat.* **2021**, *28*, 995.

[36] K. Sato, *Jpn. J. Appl. Phys.* **1981**, *20*, 2403.

[37] P. Giannozzi, S. Baroni, N. Bonini, M. Calandra, R. Car, C. Cavazzoni, D. Ceresoli, G. L. Chiarotti, M. Cococcioni, I. Dabo, A. D. Corso, S. de Gironcoli, S. Fabris, G. Fratesi, R. Gebauer, U. Gerstmann, C. Gougoussis, A. Kokalj, M. Lazzeri, L. Martin-Samos, N. Marzari, F. Mauri, R. Mazzarello, S. Paolini, A. Pasquarello, L. Paulatto, C. Sbraccia, S. Scandolo, G. Sclauzero, A. P. Seitsonen, et al., *J. Phys.: Condens. Matter* **2009**, *21*, 395502.

[38] J. P. Perdew, A. Zunger, *Phys. Rev. B* **1981**, *23*, 5048.

[39] P. E. Blöchl, *Phys. Rev. B* **1994**, *50*, 17953.